Environmental Health Engineering and Management Journal

Original Article

Environmental Health Engineering and Management

A comparative study on the adsorption of methylene blue in aqueous media by activated carbon and carbon nanosheets derived from olive stones

Negar Hariri[1,2] , Zohre Farahmandkia[2] , Esrafil Asgari[2], Hossein Danafar[3] , Mehran Mohammadian Fazli[2*]

[1]Student Research Committee, Zanjan University of Medical Sciences, Zanjan, Iran
[2]Department of Environmental Health Engineering, School of Public Health, Zanjan University of Medical Sciences, Zanjan, Iran
[3]Zanjan Pharmaceutical Biotechnology Research Center, Zanjan University of Medical Sciences, Zanjan, Iran

Abstract

Background: Olive stones, a byproduct of agricultural processes, hold significant potential for sustainable applications. In this study, activated carbon and carbon nanosheets derived from olive stones were utilized as adsorbents for removing methylene blue (MB) dye from aqueous solutions.

Methods: The preparation of activated carbon and carbon nanosheets involved grinding olive stones, followed by pyrolysis and ultrasonic treatment. The structural and morphological properties of the adsorbents were characterized using field emission scanning electron microscopy (FESEM) and transmission electron microscopy (TEM) analyses. Batch adsorption experiments were conducted to evaluate the influence of adsorbent dose, pH, initial dye concentration, and temperature on the adsorption process.

Results: Under optimized conditions, the removal efficiencies of activated carbon and carbon nanosheets were 63% and 76%, respectively, with corresponding adsorption capacities of 50.6 and 60.9 mg/g. Adsorption isotherms were well described by the Langmuir model for both adsorbents, while kinetic studies revealed conformity to the pseudo-second-order model.

Conclusion: The findings confirm that activated carbon and carbon nanosheets derived from olive stones are efficient and cost-effective adsorbents, exhibiting high adsorption capacities for MB and rapid equilibrium times in aqueous solutions.

Keywords: Olive stones, Activated carbon, Carbon nanosheets, Decolorization, Aqueous solution

Citation: Hariri N, Farahmandkia Z, Asgari E, Danafar H, Mohammadian Fazli M. A comparative study on the adsorption of methylene blue in aqueous media by activated carbon and carbon nanosheets derived from olive stones. Environmental Health Engineering and Management Journal. 2025;12:1474. doi: 10.34172/EHEM.1474.

Introduction

The textile industry is one of the major water-consuming industries, using between 25 and 250 cubic meters of water per ton of product, depending on the type of processes involved (1). Annually, more than 10 000 tons of dyes are consumed in these industries, of which 1000 tons end up in the wastewater (2). These dyes have complex structures and are released into the environment during the dyeing and finishing processes of textiles (2). The discharge of wastewater from textile industries into water bodies results in reduced sunlight penetration, decreased oxygen transfer, disruption of photosynthesis, algal blooms, and ultimately, eutrophication (3). Textile dyes possess carcinogenic and mutagenic properties, and they can cause skin allergies. Even at concentrations of less than 1.0 mg/L, the colored pollutants from these

industries can create aesthetic problems in water (4). The dyes used in the textile industry can be broadly classified into two main categories: ionic and non-ionic dyes. Ionic dyes are divided into cationic (basic) and anionic dyes (reactive, direct, and acid dyes) (5). Methylene blue (MB) is one of the most commonly used cationic dyes in the textile industry, particularly for dyeing materials such as cotton, wool, and silk. It is an aromatic heterocyclic compound with a molecular weight of 319.85 g/mol (1,6). Direct contact with this substance can cause permanent eye damage, a burning sensation at contact points, nausea and vomiting, excessive sweating, mental disturbances, and methemoglobinemia (7).

Traditional water treatment methods, including chemical coagulation, membrane filtration, and advanced oxidation processes, often face limitations

in cost, efficiency, or environmental sustainability (7). In this context, adsorption has emerged as a promising alternative due to its simplicity, cost-effectiveness, and versatility (8,9). The choice of adsorbent is crucial, and bio-based materials have gained increasing attention for their potential to provide sustainable and environmentally friendly solutions. Adsorption is a non-selective process in which a compound moves from one phase to another and accumulates in the second phase, especially when the second phase is solid. Generally, adsorption occurs through physical forces, although sometimes it can be attributed to weak chemical bonds. Adsorbents can be either organic or inorganic in nature (10). Numerous materials have been used as adsorbents for dye removal, including carbon particles, natural zeolites, mine slag, bentonite, chitosan, and agricultural waste (8,11). Many types of agricultural waste can serve as potential sources of low-cost adsorbents for removing various pollutants from aqueous solutions (12). These wastes possess high surface area, porosity, and functional groups, making them suitable for adsorption processes (13). Common agricultural wastes used as adsorbents include rice husks, banana peels, wheat straw, sugarcane bagasse, coconut shells, sawdust, date fibers, oat bran, and olive stones (12,14). These abundant, renewable, and cost-effective materials make excellent alternatives to commercial adsorbents (13,15). Additionally, their use can contribute to recycling these materials and reducing their disposal in landfills (13). The surface area and functional groups of an adsorbent play a significant role in the adsorption process. The higher the surface area and porosity, the greater the pollutant removal efficiency (16,17). To improve efficiency, nano-adsorbents are often used to remove both inorganic and organic pollutants from water and wastewater (16). The unique properties of nano-adsorbents, such as small size, catalytic potential, high reactivity, large surface area, ease of separation, and the large number of active sites for interactions with various pollutants, make them ideal materials for wastewater treatment (18). Olive stones, an agricultural byproduct abundantly generated in olive-producing regions, represent an underutilized biomass resource (19). Their conversion into value-added materials, such as activated carbon and carbon nanosheets, aligns with the principles of circular economy and waste valorization (20). These materials exhibit unique physicochemical properties, including high surface area and tunable porosity, making them ideal candidates for adsorptive removal of pollutants from aqueous solutions (20). Olive products are cultivated in regions with a Mediterranean climate, and in the past decade, there has been a significant expansion in olive orchards across various countries (21). According to a report by the FAO, several countries, including Turkey, China, Pakistan, Iran, India, and others, have implemented programs to develop olive cultivation (22). Numerous studies have utilized olive stones as an adsorbent for removing pollutants from industrial wastewater (5,23). For instance, Martin Lara used olive stones to remove chromium, copper, and nickel from electroplating wastewater (24). Other studies have employed olive stone for the removal of MB from aqueous solutions, nickel from aqueous solutions, and copper, cadmium, and lead from aqueous solutions (25-27). The primary objective of this research was to evaluate and compare the adsorption performance of activated carbon and carbon nanosheets derived from olive stones for the removal of MB from aqueous solutions. In the present study, the effects of adsorbent dose, pH, initial pollutant concentration, and temperature were also considered, along with isotherm and kinetic studies.

Materials and Methods

Materials and characterization

Olive stones are a type of agricultural/industrial waste that is readily accessible and can be collected from olive farms and olive oil industries in Tarom, Zanjan, Iran. All chemicals, including NaOH, HCl, KCl, and MB, were purchased with the highest available purity from Merck, Germany (distributed by the Research Gostaresh Zanjan Company). The shape and surface morphology of the adsorbents were analyzed using field emission scanning electron microscopy (FE-SEM, TESCAN, MIRA III) and transmission electron microscopy (TEM, CM120, Netherlands). These analyses were conducted at the Bim Gostar Taban Company, Iran.

Batch adsorption experiments

This study was conducted experimentally at a laboratory scale. To prepare the stock solution, 1.0 gram of MB powder was dissolved in deionized water and the volume was made up to 1.0 L, resulting in a concentration of 1000 mg/L. The remaining concentrations (20, 50, 100, 150, and 200 mg/L) were obtained by diluting the stock solution. Parameters were optimized using 20 mg/L of dye and 500 mg/L of adsorbent. The effects of variables such as adsorbent dose, pH, initial pollutant concentrations, and temperature on the removal of MB were investigated. Samples were placed in Falcon tubes (15 mL volume) for specified times (0 to 120 min) on a magnetic stirrer set at 100 rpm and ambient temperature. After the desired time, 1.0 mL of the solution was withdrawn using a pipette and centrifuged at 8000 rpm for 15 minutes. The remaining concentration was measured using a UV/Vis spectrophotometer (HACH model) with the supernatant solution.

To determine the optimal wavelength, the MB solution was analyzed in the spectrophotometer within the visible wavelength range (300–800 nm). Absorbance was measured at 300, 400, 500, 600, 700, and 800 nm. The highest absorbance was found to be between 600 and 700

nm, with the maximum absorbance at 663 nm. Since the absorbance in the range of 0.1-1.0 was linear, MB dye solutions with concentrations of 1.0, 2.0, 3.0, 4.0, 5.0, and 6.0 mg/L were prepared, and their absorbances were measured at 663 nm. The corresponding absorbances were 0.106, 0.152, 0.442, 0.522, 0.909, and 0.981, respectively. A standard curve was constructed using Excel, and the remaining concentration of the dye in the experimental samples was determined using the calibration equation. Samples with concentrations outside the calibration curve range were diluted. Control samples were analyzed to assess the absence of any interference between the adsorbent and MB. The pH was measured using a pH meter (Model 686, Metrohm, Switzerland), and the pH of the samples was adjusted using 0.1 N sodium hydroxide and hydrochloric acid solutions. In addition, isotherm models, kinetic models, and thermodynamic studies of the adsorption process at optimal variable values were examined for both adsorbents. To ensure the reliability of the results, all experiments were repeated three times. The percentage of dye removal and adsorption capacity (qe) were calculated using Eqs (1) and (2).

$$Removal(\%) = C0 - Ct / C0 \times 100 \qquad (1)$$

$$qe = (C0 - Ce)V / W \qquad (2)$$

Where V is the volume of solution (L), W is the mass of adsorbent (g), C_0 is the initial concentration (mg/L), C_t is the equivalent concentration (mg/L), and C_e is the equivalent concentration (mg/L).

Preparation of activated carbon and carbon nanosheets from olive stones

For the preparation of the adsorbent, the bitter olive seeds were itially washed to remove any potential contaminants. After drying, the seeds were crushed using an electric grinder, and then, boiled in 1.8 M sulfuric acid for 1.0 hour at a temperature of 60 to 80 °C to eliminate impurities (12). The treated seeds were subsequently dried in an oven at 150°C for 1 hour. The ground powder was then pyrolyzed in a vertical tube furnace (Nobertherm) under a nitrogen gas flow at a temperature of 700 °C for 2.0 hours to produce activated carbon. The activated carbon powder was then subjected to ultrasonic waves in distilled water for 1.0 hour using a 500 W ultrasonic processor equipped with a 0.5-inch diameter probe operating at a frequency of 20 kHz and an amplitude of 40% to produce carbon nanosheets. For particle size classification, standard ASTM sieves with a mesh size of 50 were used.

Results

FESEM analysis

The surface morphology and structural characteristics of the synthesized adsorbents were observed through FESEM analysis. As shown in Figures (1a) and (1b), the surface of the activated carbon adsorbent is heterogeneous, with an irregular and disordered surface, whereas the surface of the carbon nanosheets is more orderly and regular. Furthermore, examination of the images reveals that, following exposure to ultrasonic waves, the morphology of the carbon nanosheets obtained differs significantly from that of untreated activated carbon. The ultrasonic waves induce the fragmentation of activated carbon particles into smaller sizes and their dispersion in the liquid medium, leading to the synthesis of carbon nanosheets (28). This process results in the formation of carbon nanosheets with an expanded surface area, which can potentially be utilized in applications such as energy storage and conversion, catalysis, and water purification. The FESEM analysis results show particle sizes ranging from 100 to 150 nm for activated carbon and 80 to 100 nm for the carbon nanosheets.

TEM analysis

TEM analysis is a powerful technique that provides valuable insights into the morphology and surface structure of adsorbents such as activated carbon and carbon nanosheets. As shown in Figures 2a and 2b, the TEM analysis reveals that activated carbon has an
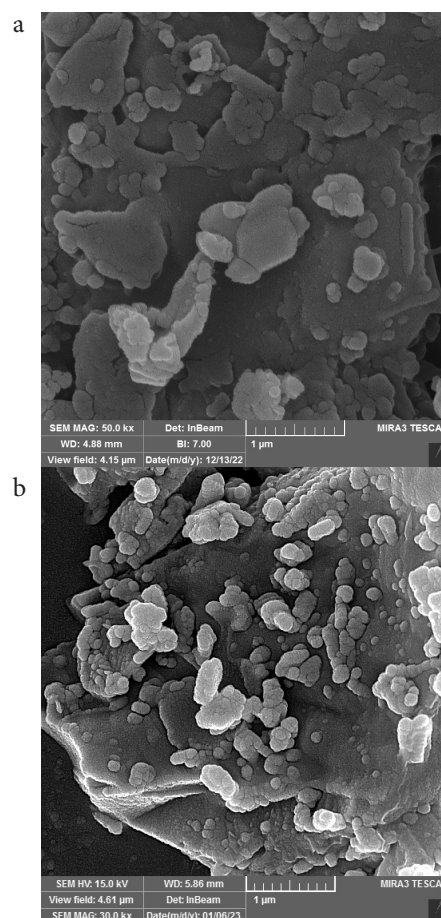

Figure 1. FESEM analysis of activated carbon (a) and carbon nanosheets (b)

amorphous structure with irregular pores and a disordered arrangement of carbon atoms, which contribute to its excellent adsorption properties. In contrast, carbon nanosheets consist of thin graphene layers that are only a few nanometers thick. They exhibit a well-defined two-dimensional structure with a significant aspect ratio and remarkable mechanical, electrical, and thermal properties (28). TEM analysis shows that carbon nanosheets have a flat and orderly structure with a hexagonal arrangement of carbon atoms. This unique atomic arrangement in carbon nanosheets imparts exceptional properties, making them ideal for a wide range of applications such as energy storage, catalysis, and electronics.

Operating variables effect
Effect of contact time
Examining the effect of time across different intervals (25, 45, 65, 85, 105, and 120 minutes) reveals that variations in removal efficiency and adsorption capacity differ between the two adsorbents, each following a distinct pattern over time (Figures 3a and 3b).

As shown in Figure 3a, the removal efficiency and adsorption capacity of MB on activated carbon increase steadily with time, reaching their peak at 120 minutes. At this point, the removal efficiency reaches 63%, and the adsorption capacity is 50.6 mg/g.

For carbon nanosheets, Figure 3b indicates that the removal efficiency and adsorption capacity of MB reach maximum values at 45 minutes, with removal efficiency of 76% and adsorption capacity of 60.9 mg/g.
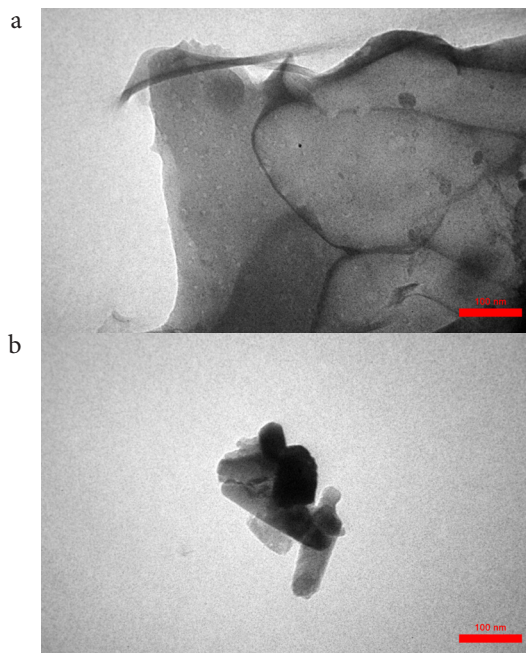
Effect of temperature

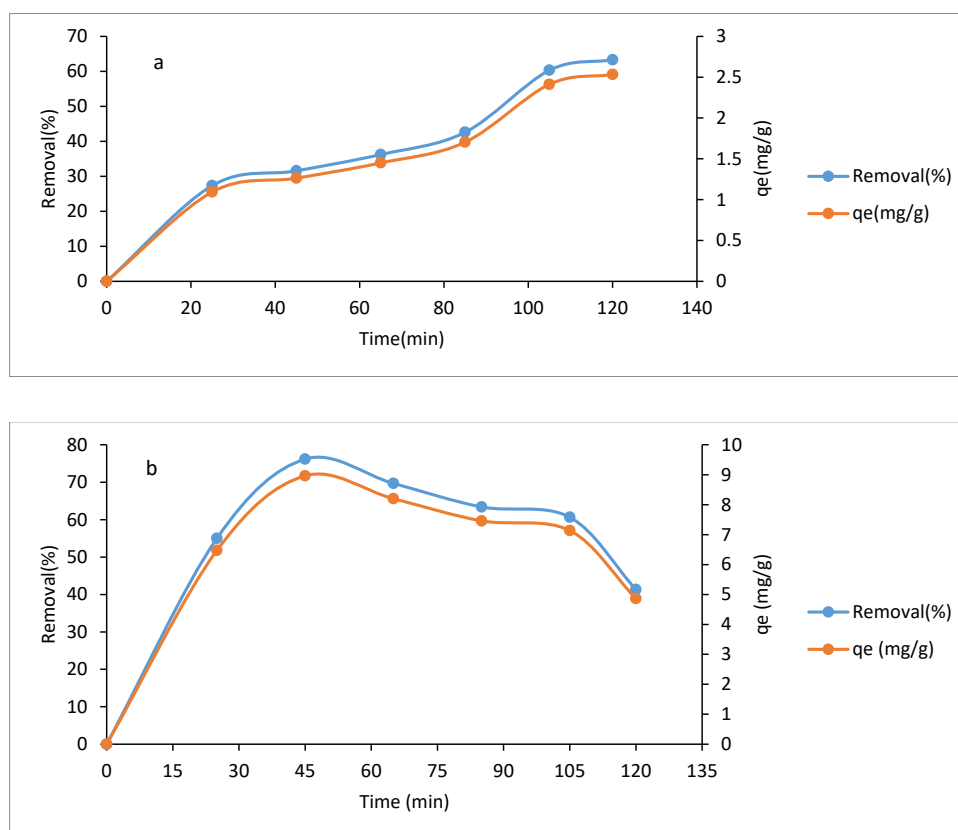**Figure 2.** TEM analysis of activated carbon (a) and carbon nanosheets (b)

Figure 3. The contact time effect for activated carbon (a) and carbon nanosheets (b). (pH = 7.0, temperature = 25 ℃, dye concentration = 20 mg/L, and adsorbent dose = 250 mg/L)
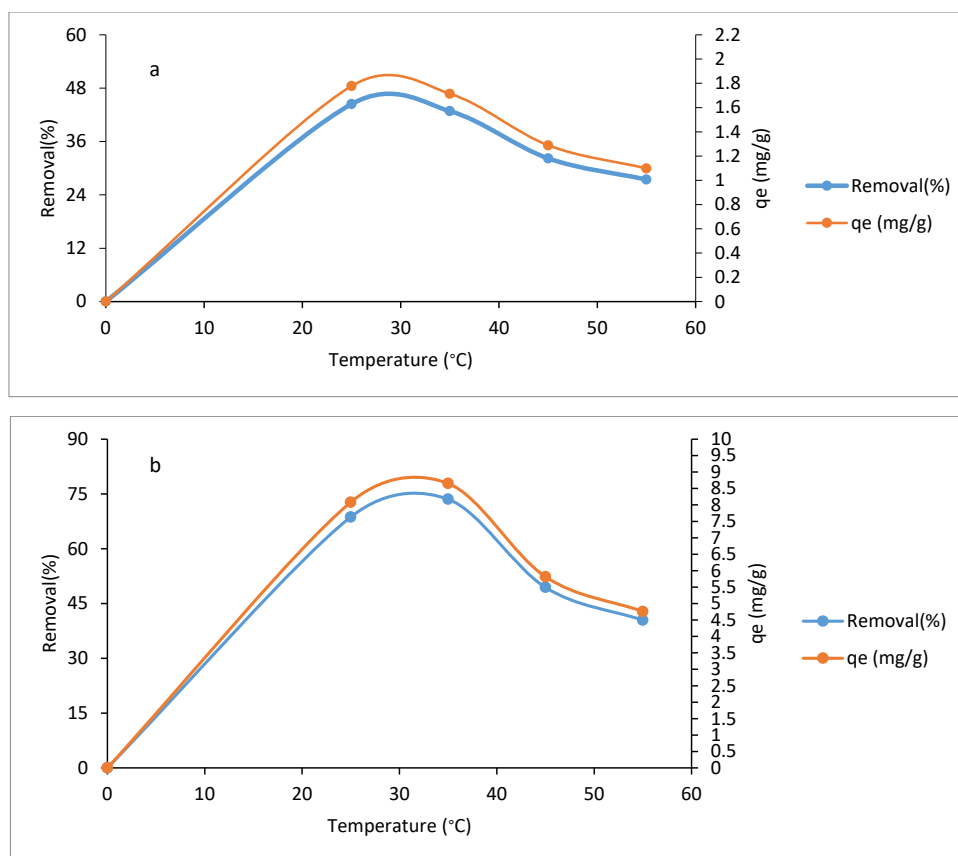
Figure 4. The temperature effect for activated carbon (a) and carbon nanosheets (b). (pH = 7.0, contact time = 120 min for activated carbon and 45 min for carbon nanosheets, dye concentration = 20 mg/L, and adsorbent dose = 250 mg/L)

The impact of temperature on the removal efficiency and adsorption capacity of MB on activated carbon and carbon nanosheets is illustrated in Figures 4a and 4b.

As seen in Figure 4a, the removal efficiency and adsorption capacity of MB on activated carbon reach their maximum at the lowest temperature (25 °C), where the removal efficiency is 44%, and the adsorption capacity is 35.55 mg/g. As the temperature increases from 25 to 55 °C, both removal efficiency and adsorption capacity decrease, reaching 27% and 21.96 mg/g, respectively.

For carbon nanosheets, as shown in Figure 4b, the highest removal efficiency and adsorption capacity are observed at 35 °C, with values of 74% and 58.8 mg/g, respectively. However, as the temperature increases from 35 to 55 °C, both removal efficiency and adsorption capacity decrease to 40% and 32.3 mg/g, respectively.

Effect of pH
The influence of varying pH levels (3.0, 5.0, 7.0, and 10) on the removal efficiency and adsorption capacity of MB on activated carbon and carbon nanosheets is illustrated in Figures 5a and 5b. According to Figure 5a, in activated carbon, as pH increases from 3.0 to 10, both removal efficiency and adsorption capacity for MB increase steadily.

As shown in Figure 5b, the removal efficiency of MB on carbon nanosheets increases significantly with rising pH.

At pH 3.0, the removal efficiency is around 39%, whereas it rises to 79% at pH 10. Furthermore, the adsorption capacity of MB on carbon nanosheets also steadily increases with pH, from 31.4 mg/g at pH 3.0 to 63.6 mg/g at pH 10.

Effect of initial dye concentration
The effect of initial MB concentration on its removal efficiency and adsorption capacity on activated carbon and carbon nanosheets is illustrated in Figures 6a and 6b.

As shown in Figure 6a, the removal efficiency of MB on activated carbon decreases substantially with an increase in its initial concentration from 20 to 200 mg/L.

Similarly, for carbon nanosheets, an increase in the initial concentration of MB results in a decline in removal efficiency and variations in adsorption capacity, as depicted in Figure 6b. In this case, the removal efficiency decreases from 74% to 5.0% as the concentration rises from 20 to 200 mg/L.

Effect of adsorbent dose
Analysis of the results from Figures 7a and 7b at varying adsorbent dosages (20, 60, 120, 250, and 550 mg/L) demonstrates an inverse relationship in the behavior of removal efficiency and adsorption capacity with increased adsorbent dosage.
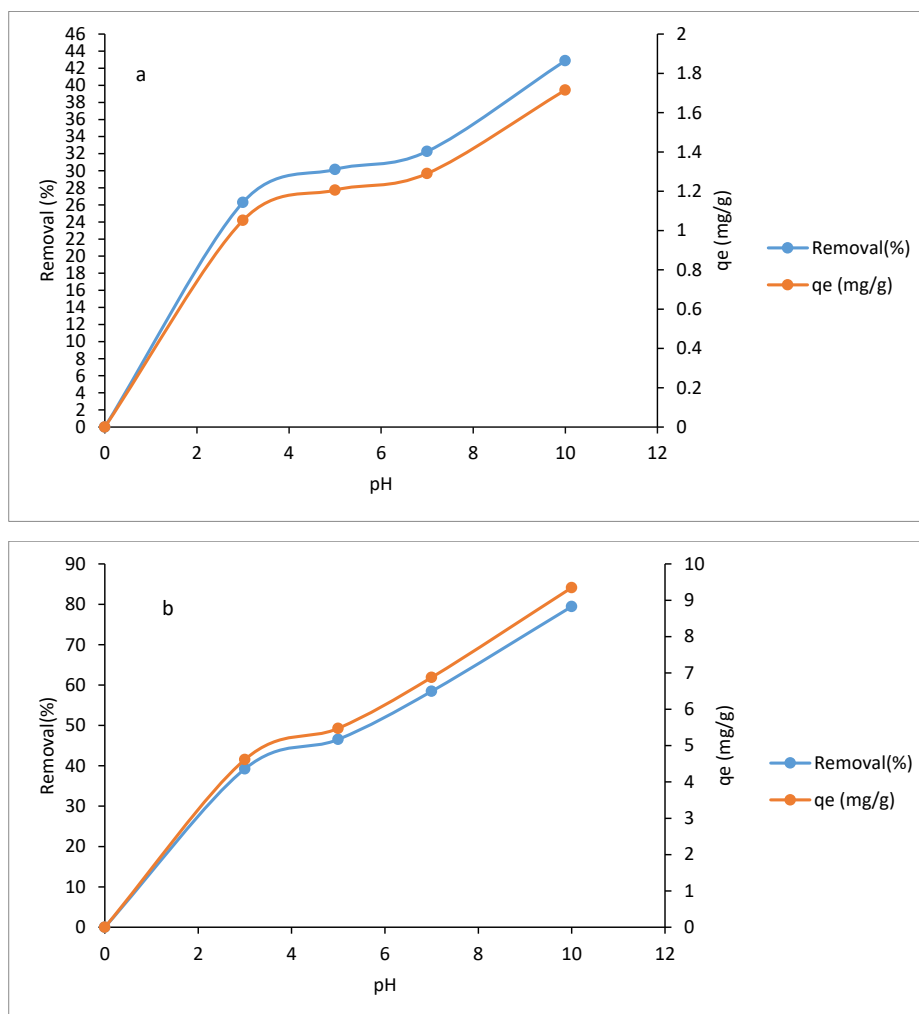
Figure 5. The pH effect for activated carbon (a) and carbon nanosheets (b). (temperature=25ºC for activated carbon and 35 ºC for carbon nanosheets, contact time=120 min for activated carbon and 45 min for carbon nanosheets, dye concentration=20 mg/L, and adsorbent dose=250 mg/L)

For activated carbon, Figure 7a shows that increasing the adsorbent dosage from 20 to 550 mg/L leads to a significant increase in MB removal efficiency.

A similar trend is observed for carbon nanosheets. As shown in Figure 7b, increasing the adsorbent dosage from 20 to 550 mg/L increases the MB removal efficiency from 20% to 81%.

Isotherm studies
In this study, the equilibrium adsorption data were analyzed using Langmuir, Freundlich, Temkin, and Dubinin-Radushkevich models to identify the most suitable adsorption model for the different adsorbents (Table S1).

The results in Table 1 indicate that the correlation coefficients (R^2) for the Langmuir isotherm model for activated carbon and carbon nanoplates are 0.92 and 0.99, respectively, demonstrating a better fit of the data to this model compared to the other models. These findings suggest that the Langmuir isotherm model is more suitable for describing the MB adsorption process on both adsorbents. Figures S1 and S2, presented separately

for activated carbon and carbon nanoplates, show good alignment with the Langmuir isotherm model.

Adsorption kinetics
To calculate the kinetics of the data, pseudo-first-order and pseudo-second-order kinetics were performed according to Figure S3, and the results were entered in Table 2 for both activated carbon adsorbents and activated carbon nanosheets. According to the results obtained from Figure S3 and Table 2, due to the high correlation coefficient for MB adsorption on these two adsorbents, the second-order pseudo-kinetic model was identified as the more appropriate model.

Thermodynamic study
Figure S4 and Table 3 show the results of thermodynamic calculations of two adsorbents, activated carbon and activated carbon nanosheets.

Discussion
Operating variables effect
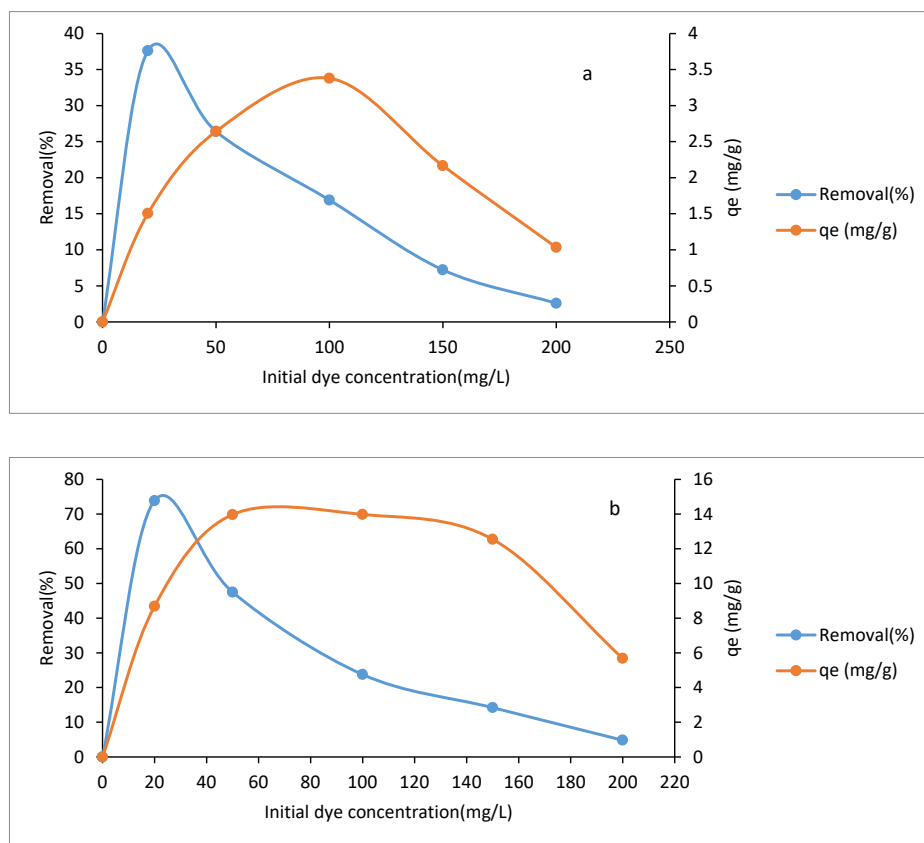### Effect of contact time

Figure 6. The initial dye concentration effect for activated carbon (a) and carbon nanosheets (b). (pH = 7.0, temperature = 25°C for activated carbon and 35 °C for carbon nanosheets, contact time = 120 min for activated carbon and 45 min for carbon nanosheets, and adsorbent dose = 250 mg/L)
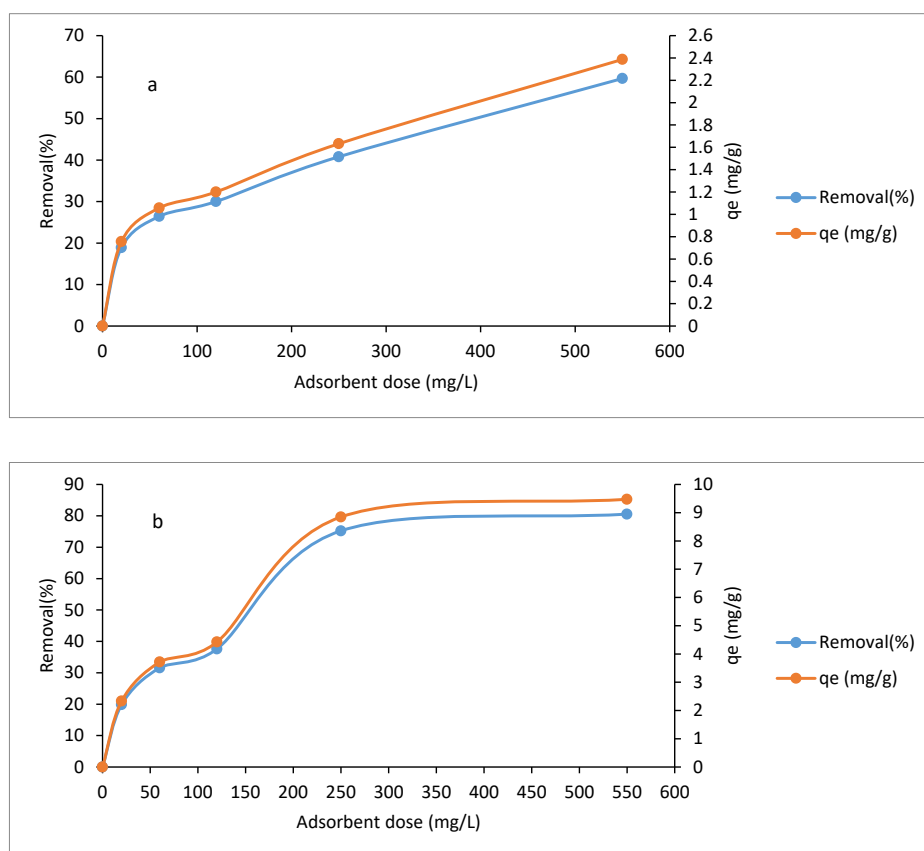

Figure 7. The adsorbent dose effect for activated carbon (a) and carbon nanosheets (b). (pH = 10, temperature = 25 °C for activated carbon and 35 °C for carbon nanosheets, contact time = 120 min for activated carbon and 45 min for carbon nanosheets, and dye concentration = 20 mg/L)

Table 1. Correlation coefficient of isotherm models

Adsorbents	Isotherm models			
	Langmuir	Freundlich	Temkin	Dubinin-Radushkevich
Activated carbon	$R^2 = 0.92$	$R^2 = 0.49$	$R^2 = 0.44$	$R^2 = 0.70$
Carbon nanosheets	$R^2 = 0.99$	$R^2 = 0.61$	$R^2 = 0.56$	$R^2 = 0.57$

Table 2. Kinetic models correlation coefficients

Adsorbents	Pseudo-first-order	Pseudo-second-order
Activated carbon	$R^2 = 0.96$	$R^2 = 0.98$
Carbon nanosheets	$R^2 = 0.96$	$R^2 = 0.99$

Table 3. Thermodynamic parameters

Adsorbents	Parameters	
	ΔH° (KJ/mol)	ΔS° (J/mol.K)
Activated carbon	-21841	-88
Carbon nanosheets	-36748	-119

Contact time is a critical factor in the adsorption process, significantly influencing the removal efficiency and adsorption capacity of pollutants like MB on adsorbents such as activated carbon and carbon nanosheets (29). As shown in Figure 3a, the gradual increase suggests that at the initial stages of adsorption, a large number of active sites are available on the activated carbon surface, allowing MB molecules to be readily adsorbed. Over time, as more of these active sites are occupied, the adsorption process approaches equilibrium, leading to a plateau as most of the active sites become saturated.

As shown in Figure 3b, the rapid increase demonstrates that carbon nanosheets offer a high surface area and numerous active sites for adsorption in the initial stages. However, beyond the 45-minute mark, a gradual decline in removal efficiency and adsorption capacity occurs, ultimately reaching 41% and 33.1 mg/g, respectively, at 120 min. This decrease may be attributed to several factors, including competition among MB molecules for the remaining active sites and desorption of previously adsorbed molecules due to a dynamic equilibrium between the adsorbed phase and the solution phase. In other words, as time progresses, some molecules desorb from the adsorbent surface, re-entering the solution.

With activated carbon, a longer contact time (120 minutes) results in the maximum removal efficiency and adsorption capacity, as adsorption continuously increases until this point. This behavior suggests a slower adsorption process approaching equilibrium over time (30). In contrast, for carbon nanosheets, adsorption quickly reaches its peak at 45 minutes, followed by a gradual decrease in removal efficiency and adsorption capacity, which may be due to desorption or a reduction in available active sites (30). Therefore, these findings highlight the importance of optimal contact time in the

adsorption process. Selecting an appropriate contact time can achieve maximum removal efficiency and adsorption capacity, avoiding resource waste. For activated carbon, a longer contact time is more effective, while shorter times are preferable for carbon nanosheets.

Effect of temperature
Temperature is a crucial factor in adsorption processes, as it influences the energy distribution of adsorbate and adsorbent molecules as well as their interactions (12). By examining the effects of temperature at various levels (25, 35, 45, and 55 °C) on the removal efficiency and adsorption capacity of MB on activated carbon and carbon nanosheets, it is possible to analyze the differing behavior of these adsorbents at different temperatures (12).

As shown in Figures 4a and 4b, the reduction of the removal efficiency and the adsorption capacity with the temperature increase may indicate a physical adsorption process dominated by weak intermolecular forces such as van der Waals forces. In physical adsorption, the pollutant molecules bind to the adsorbent through van der Waals interactions; as temperature increases, the kinetic energy of molecules also increases, causing them to desorb more readily from the adsorbent surface, leading to decreased removal efficiency and adsorption capacity. The similarity in adsorption capacities can be attributed to the high surface area and porosity of bio-based adsorbents, which facilitate effective pollutant uptake. However, the slightly higher adsorption capacity of carbon nanosheets compared to activated carbon in this study may be explained by their unique layered structure, offering enhanced accessibility to active sites. Therefore, the findings indicate that the adsorption process of MB on activated carbon and carbon nanosheets is more efficient at lower temperatures (2). The decrease in removal efficiency and adsorption capacity at higher temperatures, especially for physical adsorption processes, is due to increased molecular kinetic energy, reducing the stability of the weak van der Waals bonds between the pollutant molecules and the adsorbent surface (2). Therefore, lower temperatures appear more suitable for optimizing MB adsorption on these adsorbents. These results also highlight the importance of temperature control in adsorption systems. At lower temperatures, removal efficiency and adsorption capacity increase, which can be advantageous for industrial and environmental applications, offering higher efficiency and energy savings.

Effect of pH
pH plays a crucial role in determining removal efficiency and adsorption capacity, as it affects the surface charge of the adsorbent and the degree of ionization of pollutants (31). The effect of pH on adsorption processes is a significant factor that can greatly influence the removal efficiency and adsorption capacity of pollutants such

as MB on adsorbents like activated carbon and carbon nanosheets (31). The pH of the solution can modulate interactions between the adsorbent and pollutant by altering the surface charge of the adsorbent and the degree of ionization of pollutant molecules.

According to Figure 5a, at lower pH levels, due to greater protonation of the activated carbon surface, there is heightened competition between hydrogen ions (H^+) and MB molecules for adsorption sites. This situation results in a reduced removal efficiency at pH 3.0, where the removal efficiency is approximately 26%. As the pH increases, the number of negatively charged sites on the activated carbon surface increases, promoting the adsorption of the positively charged MB molecules. Consequently, the removal efficiency at pH 10 reaches 43%. Additionally, the adsorption capacity of MB on activated carbon increases from 21.04 mg/g at pH 3.0 to 34.31 mg/g at pH 10. This increase suggests that at higher pH levels, the competition from H^+ ions diminishes, and the adsorbent's affinity for MB improves, leading to an increase in adsorption capacity. A similar trend is observed for carbon nanosheets.

According to Figure 5a, the increase is due to the heightened negative charge on the carbon nanosheet surface at higher pH levels, enhancing electrostatic interactions between the adsorbent surface and MB. This increase in adsorption capacity at higher pH levels is due to the adsorbent's increased affinity for MB and reduced competition from hydrogen ions, enabling the adsorbent to accommodate more MB molecules on its surface. At lower pH levels, competition from hydrogen ions and a decrease in the adsorbent's negative surface charge reduce MB adsorption. In contrast, at higher pH levels, the increase in negative surface charge of the adsorbent enhances MB adsorption due to stronger electrostatic interactions between the adsorbent and pollutant (32). Therefore, it can be concluded that optimal conditions for MB adsorption occur at higher pH levels, where both removal efficiency and adsorption capacity reach their maximum values.

Effect of initial dye concentration

The initial concentration of MB significantly affects its removal efficiency and adsorption capacity on adsorbents like activated carbon and carbon nanosheets due to differences in surface properties and adsorption behavior (33). Examining this phenomenon at varying MB concentrations (20, 50, 100, 150, and 200 mg/L) reveals distinct trends in removal efficiency and adsorption capacity as the initial concentration increases.

According to Figure 6a, this decrease, especially at higher concentrations, is due to the rapid saturation of the activated carbon surface. For example, at 20 mg/L, the removal efficiency is around 38%, but it drops to 3.0% as the concentration increases. On the other hand, the

adsorption capacity of MB on activated carbon initially rises with an increase in initial concentration from 20 to 100 mg/L, reaching 30.08 to 67.6 mg/g. However, at concentrations above 100 mg/L, the adsorption capacity decreases, reaching 20.67 mg/g at 200 mg/L. These changes highlight the saturation limits of the activated carbon surface and the reduction of available space for further adsorption of MB molecules.

According to Figure 6b, this downward trend is caused by the limited number of active adsorption sites on the carbon nanosheets at higher concentrations. Additionally, the adsorption capacity of carbon nanosheets shows an increasing trend from 20 to 100 mg/L, reaching 59.11 to 95.07 mg/g, but then declines to 38.67 mg/g as the concentration reaches 200 mg/L. This reduction in adsorption capacity is also due to the saturation of the nanosheet surface and the decrease in the number of vacant adsorption sites.

At lower MB concentrations, both adsorbents exhibit higher adsorption capacities and removal efficiencies, which can be attributed to a greater number of free adsorption sites on the adsorbent surfaces (33,34). As the concentration increases, competition among MB molecules for adsorption intensifies, leading to surface saturation, making it increasingly challenging to adsorb new molecules (34). Ultimately, this saturation effect results in a reduction in removal efficiency and a relative decrease in adsorption capacity (35).

Effect of adsorbent dose

Adsorbent dosage is considered a crucial factor in adsorption processes (36,37). The effect of adsorbent dosage on the removal efficiency and adsorption capacity of MB by adsorbents such as activated carbon and carbon nanosheets is of particular significance due to the structural and surface property differences between these adsorbents.

According to Figure 7a, this increase is due to the greater number of active sites available at higher adsorbent dosages, which are more accessible to MB molecules. Consequently, the removal efficiency increases from 19% at 20 mg/L dosage to 60% at 550 mg/L. On the other hand, the adsorption capacity of activated carbon decreases with higher dosages, dropping from an initial 189 mg/g at 20 mg/L to 21.7 mg/g at 550 mg/L. This reduction in adsorption capacity per unit mass of adsorbent can be attributed to a more uniform distribution of MB molecules across a larger adsorbent surface and a decrease in equilibrium concentration of the adsorbate, which reduces adsorption per unit mass.

According to Figure 7b, this improvement is due to the availability of more active sites for MB adsorption at higher adsorbent dosages. However, the adsorption capacity of carbon nanosheets decreases with increasing adsorbent dosage, from 198.5 mg/g at 20 mg/L to 29.28

mg/g at 550 mg/L. The cause of this decrease, similar to that for activated carbon, lies in the reduced equilibrium concentration of the adsorbate and its more uniform distribution across a larger adsorbent surface.

Therefore, increasing the adsorbent dosage enhances removal efficiency due to a greater number of active adsorption sites accessible to MB molecules (36). However, the adsorption capacity per unit mass of adsorbent decreases because, as dosage increases, equilibrium concentration lowers and MB molecules are distributed across a larger adsorbent surface (36,38). This interplay between removal efficiency and adsorption capacity indicates that the optimal adsorbent dosage should be carefully selected based on the intended application and pollutant solution characteristics to maximize removal efficiency and effective adsorption capacity.

Isotherm studies

To determine the maximum adsorption capacity, which is one of the key parameters in the design and evaluation of adsorption processes, equilibrium adsorption isotherms were investigated (39). Equilibrium adsorption isotherms represent the relationship between the concentration of the pollutant in the solution and the amount adsorbed onto the surface of the adsorbent at equilibrium conditions. These isotherms can predict adsorption behavior under various conditions and assist in the design of adsorption systems.

The Langmuir isotherm model is one of the most well-known and widely used models for describing surface adsorption processes (38). This model assumes that the adsorption of molecules onto the adsorbent surface occurs as a monolayer under equilibrium conditions. In other words, each adsorbed molecule occupies only one adsorption site, and there are no mutual interactions between the adsorbed molecules on the surface (7). The model is based on the assumption that the adsorbent surface is homogeneous, with all adsorption sites being energetically identical. Additionally, in the Langmuir model, adsorption is considered reversible, meaning that adsorbed molecules can detach from the adsorbent surface, but under normal conditions, the process reaches equilibrium (34).

Along with the Langmuir isotherm model, other models such as the Freundlich, Temkin, and Dubinin-Radushkevich isotherms are also used to describe the adsorption process (18). These models may be more suitable for specific conditions or heterogeneous adsorbents. The Freundlich model is typically applied to adsorbents where adsorption occurs in multiple layers or in a non-homogeneous manner (4). The Dubinin-Radushkevich model, on the other hand, is ideal for studying adsorption processes on porous adsorbents and describing the penetration of molecules into the pores of the structure (4).

According to Figures S1 and S2, these results indicate that the MB adsorption process on both adsorbents occurs in a monolayer and homogeneous manner, where the adsorbent surface is fully occupied at equilibrium. This suggests excellent performance of these adsorbents in removing harmful dyes from aqueous solutions, particularly in situations where the adsorption process needs to occur rapidly and at high capacities. Given the high correlation coefficient (0.99) for the Langmuir model, these adsorbents can be effectively employed in water and wastewater treatment processes.

Adsorption kinetics

The first-order and second-order pseudo-kinetic models (Eqs (3) and (4)) are mathematical models used to describe the rate of chemical reactions (40). These models are particularly useful for analyzing the behavior of reactions and predicting outcomes in various processes, especially in the field of adsorption from aqueous solutions (40). Specifically, in adsorption processes, these models are applied to analyze the rate of pollutant adsorption, such as dyes, onto adsorbents.

Pseudo-first order:

$$Ln(q_e - q_t) = Lnq_e - k_1 t \qquad (3)$$

Pseudo-second order:

$$\frac{t}{q_t} = \frac{1}{k_2 q_e^2} + \frac{1}{q_e} t \qquad (4)$$

Where q_t (mg/g) is the adsorption at time t (min); q_e (mg/g) is the adsorption capacity at adsorption equilibrium; and k_1 (1/min), and k_2 (g/mg.min) are the kinetic rate constants for the pseudo-first-order and pseudo-second-order models, respectively.

The first-order pseudo-kinetic model is a simple model that assumes the adsorption rate is linearly related to the concentration of the adsorbed molecules on the adsorbent surface (41). This model is suitable for systems where the adsorption process follows a simple molecular exchange pattern. On the other hand, the second-order pseudo-kinetic model is a more complex model, particularly applicable to adsorption processes where the reaction rate is significantly dependent on the concentrations of adsorbed species on the adsorbent surface (42). This model assumes that adsorption occurs rapidly at first and gradually slows down as the system approaches equilibrium (42). In Figure S3, it can be observed that over time, the adsorption gradually approaches equilibrium, with the adsorption rate being higher in the initial stages compared to the final stages. In other words, the adsorption of MB onto activated carbon and carbon nanosheets follows a more complex kinetic pattern, where the adsorption process initially occurs rapidly, and then, gradually proceeds towards equilibrium.

Thermodynamic study

Thermodynamics of adsorption is a crucial tool for understanding and analyzing surface adsorption processes (32). In this context, the effect of temperature on the MB adsorption process onto activated carbon and carbon nanosheets can be fully explained from a thermodynamic perspective. Based on the thermodynamic data obtained in this study (Figure S4 and Table 3), it can be concluded that the adsorption of MB onto both activated carbon and carbon nanosheets is a spontaneous and exothermic process, in which energy is released with increasing temperature. Additionally, the negative value of the adsorption entropy indicates that the adsorption process is associated with an increase in order at the surface of the adsorbent. These results highlight the high efficiency and potential of these adsorbents in the removal of dyes and pollutants in water and wastewater treatment processes. The adsorption of MB onto these adsorbents is a physical adsorption process, in which physical forces such as van der Waals forces and surface interactions play the primary role. This implies that the adsorption energy is low, and the adsorbent-adsorbate interactions primarily result from van der Waals forces. The thermodynamic parameters that describe the adsorption process include Gibbs free energy ($\Delta G°$), enthalpy ($\Delta H°$), and entropy ($\Delta S°$) (Eqs. (5) and (7)).

$$Kd = qe / Ce \tag{5}$$

$$Ln\,kd = \Delta S° / R - \Delta H° / RT \tag{6}$$

$$\Delta G° = -RT\,Ln\,kd \tag{7}$$

Where R is the universal gas constant (8314 J/mol·K) and kd (1/g) is the ratio of the amount of dye adsorbed onto the adsorbent (mg/g) to the remaining concentration of dye in the solution (mg/L).

Comparison of adsorbents in this study with previous research

Table S2 presents a comparison between previous studies and the present research on the removal of MB using various adsorbents. Despite differences in operational conditions, comparing the adsorption capacities of these adsorbents with those obtained in the present work can reveal whether carbon-based adsorbents derived from olive stone offer exceptional performance. This comparison considers factors such as maximum adsorption capacity, removal efficiency, contact time, and adsorbent dosage. The results from this comparison indicate that the adsorption capacity obtained in this study shows improved performance compared to some previous research, while being slightly lower in others. Therefore, it reflects the high efficacy of carbon-based

adsorbents derived from olive stone for MB removal. Key factors influencing dye adsorption include the adsorbent's specific surface area, pore size and shape, and chemical interactions between MB molecules and the adsorbent surface (23). The structure of carbon nanosheets derived from olive pits, due to their unique structural features such as high surface area and nanoscale porous structure, provides favorable conditions for efficient adsorption (5). The adsorption capacities of activated carbon and carbon nanosheets derived from olive stones for MB are consistent with several studies using bio-based adsorbents. For instance, materials derived from agricultural residues such as coconut shells, rice husks, and fruit peels have demonstrated comparable performance in terms of dye removal efficiency (43). Discrepancies with other studies, where specific adsorbents exhibit higher or lower capacities, may arise from variations in preparation methods, surface functionalization, or experimental conditions, such as initial dye concentration and pH (44). For example, pyrolysis temperature and activation processes significantly influence the development of micropores and surface chemistry, which are critical factors in adsorption (45).

Conclusion

The morphology and properties of the studied adsorbents (activated carbon and carbon nanosheets) were characterized by FESEM and TEM analyses. These adsorbents were used for the removal of MB in batch adsorption experiments, and the effects of parameters such as adsorbent dose, pH, initial contaminant concentration, and temperature on the removal of MB were investigated. Analysis of the experimental data using Langmuir, Freundlich, and Temkin isotherms reveals that the equilibrium data for both adsorbents best fit the Langmuir model. The kinetic process also successfully followed the pseudo-second-order kinetic model for both adsorbents. Under optimal conditions, the removal efficiency and adsorption capacity for activated carbon and carbon nanosheets were 63% and 76%, and 50.6 and 60.9 mg/g, respectively. Based on the results, the activated carbon and carbon nanosheets synthesized from olive pits are cost-effective and environmentally friendly adsorbents, and are considered efficient materials for the removal of MB from aqueous solutions. Therefore, the findings of the present study contribute to expanding our knowledge of the application of bio-based and environmentally compatible materials for the removal of pollutants from aqueous solutions. These materials offer a sustainable approach for water purification and can effectively reduce contamination caused by industrial dyes. This approach holds promise as a viable solution for addressing pollution issues and improving water treatment practices.

Authors' contributions

Conceptualization: Mehran Mohammadian Fazli.
Data curation: Negar Hariri.
Formal analysis: Negar Hariri and Esrafil Asgari.
Funding acquisition: Mehran Mohammadian Fazli, Negar Hariri.
Investigation: Mehran Mohammadian Fazli, Zohre Farahmandkia.
Methodology: Mehran Mohammadian Fazli, Zohre Farahmandkia.
Project administration: Mehran Mohammadian Fazli, Negar Hariri.
Supervision: Mehran Mohammadian Fazli.
Validation: Hossein Danafar.
Visualization: Hossein Danafar and Negar Hariri.
Writing–original draft: Negar Hariri.
Writing–review & editing: Esrafil Asgari.

Competing interests

The authors declare that they have no conflict of interests regarding the publication of the present article.

Ethical issues

Not applicable.

Funding

Not applicable.

Supplementary files

Supplementary file 1 contains Figure S1-S4 and Tables S1-S2.

References

1. Vajnhandl S, Valh JV. The status of water reuse in European textile sector. J Environ Manage. 2014;141:29-35. doi: 10.1016/j.jenvman.2014.03.014.
2. Maheshwari K, Agrawal M, Gupta AB. Dye pollution in water and wastewater. In: Novel Materials for Dye-containing Wastewater Treatment. Singapore: Springer; 2021. p. 1-25. doi: 10.1007/978-981-16-2892-4_1.
3. Ghaly AE, Ananthashankar R, Alhattab M, Ramakrishnan VV. Production, characterization and treatment of textile effluents: a critical review. J Chem Eng Process Technol. 2014;5(1):182. doi: 10.4172/2157-7048.1000182.
4. Ozcan DO, Hendekci MC, Ovez B. Enhancing the adsorption capacity of organic and inorganic pollutants onto impregnated olive stone derived activated carbon. Heliyon. 2024;10(12):e32792. doi: 10.1016/j.heliyon.2024.e32792.
5. Wafaa Y, Akazdam S, Zyade S, Chafiq M, Gun Ko Y, Chafi M, et al. Mechanistic insights into methylene blue removal via olive stone-activated carbon: a study on surface porosity and characterization. J Saudi Chem Soc. 2023;27(5):101692.

6. doi: 10.1016/j.jscs.2023.101692.
7. Soubh AM, Abdoli MA, Ahmad LA. Optimizing the removal of methylene blue from aqueous solutions using persulfate activated with nanoscale zero valent iron (nZVI) supported by reduced expanded graphene oxide (rEGO). Environ Health Eng Manag. 2021;8(1):15. doi: 10.34172/ehem.2021.03.
8. Katheresan V, Kansedo J, Lau SY. Efficiency of various recent wastewater dye removal methods: a review. J Environ Chem Eng. 2018;6(4):4676-97. doi: 10.1016/j.jece.2018.06.060.
9. Crini G, Lichtfouse E, Wilson LD, Morin-Crini N. Adsorption-oriented processes using conventional and non-conventional adsorbents for wastewater treatment. In: Crini G, Lichtfouse E, eds. Green Adsorbents for Pollutant Removal: Fundamentals and Design. Cham: Springer; 2018. p. 23-71. doi: 10.1007/978-3-319-92111-2_2.
10. Rami Y, Shoshtari-Yeganeh B, Ebrahimi A, Ebrahimpour K. Occurrence and characteristics of microplastics in surface water and sediment of Zayandeh-Rud river, Iran. Environ Health Eng Manag. 2023;10(2):207. doi: 10.34172/ehem.2023.23.
11. Iwuozor KO, Akpomie KG, Conradie J, Adegoke KA, Oyedotun KO, Ighalo JO, et al. Aqueous phase adsorption of aromatic organoarsenic compounds: a review. J Water Process Eng. 2022;49:103059. doi: 10.1016/j.jwpe.2022.103059.
12. Shahsavani E, Ehrampoush MH, Samaei MR, Abouee Mehrizi E, Madadizadeh F, Abbasi A, et al. Performance evaluation of the combined process of ozonation, biological activated carbon reinforced by bacterial consortium, and ultrafiltration in greywater treatment. Environ Health Eng Manag. 2022;9(4):381. doi: 10.34172/ehem.2022.41.
13. Dai Y, Sun Q, Wang W, Lu L, Liu M, Li J, et al. Utilizations of agricultural waste as adsorbent for the removal of contaminants: a review. Chemosphere. 2018;211:235-53. doi: 10.1016/j.chemosphere.2018.06.179.
14. Ramaraju B, Manoj Kumar Reddy P, Subrahmanyam C. Low cost adsorbents from agricultural waste for removal of dyes. Environ Prog Sustain Energy. 2014;33(1):38-46. doi: 10.1002/ep.11742.
15. Omidinasab M, Rahbar N, Ahmadi M, Kakavandi B, Ghanbari F, Kyzas GZ, et al. Removal of vanadium and palladium ions by adsorption onto magnetic chitosan nanoparticles. Environ Sci Pollut Res Int. 2018;25(34):34262-76. doi: 10.1007/s11356-018-3137-1.
16. Teymouri P, Jaafarzadeh N, Mostoufi A, Amiri H, Alavi N, Dinarvand M, et al. Effect of pretreatment on *Ceratophyllum demersum* for enhanced biosorption of Cr(VI) and Cd(II). Environ Eng Manag J. 2017;16(2):459-69.
17. Ali I, Asim M, Khan TA. Low cost adsorbents for the removal of organic pollutants from wastewater. J Environ Manage. 2012;113:170-83. doi: 10.1016/j.jenvman.2012.08.028.
18. Malakootian M, Faraji M, Malakootian M, Nozari M. Ciprofloxacin removal from aqueous media by adsorption process: a systematic review and meta-analysis. Desalin Water Treat. 2021;229:252-82. doi: 10.5004/dwt.2021.27334.
19. Varsha M, Senthil Kumar P, Senthil Rathi B. A review on recent trends in the removal of emerging contaminants from aquatic environment using low-cost adsorbents. Chemosphere. 2022;287(Pt 3):132270. doi: 10.1016/j.chemosphere.2021.132270.
20. Anvari S, Aguado R, Jurado F, Fendri M, Zaier H, Larbi A, et al. Analysis of agricultural waste/byproduct biomass potential for bioenergy: the case of Tunisia. Energy Sustain

Dev. 2024;78:101367. doi: 10.1016/j.esd.2023.101367.

20. Skaltsounis AL, Argyropoulou A, Aligiannis N, Xynos N. Recovery of high added value compounds from olive tree products and olive processing byproducts. In: Boskou D, ed. Olive and Olive Oil Bioactive Constituents. AOCS Press; 2015. p. 333-56. doi: 10.1016/b978-1-63067-041-2.50017-3.

21. Fraga H, Pinto JG, Viola F, Santos JA. Climate change projections for olive yields in the Mediterranean Basin. Int J Climatol. 2020;40(2):769-81. doi: 10.1002/joc.6237.

22. Özdel MM, Ustaoğlu B, Cürebal İ. Modeling of the potential distribution areas suitable for olive (Olea europaea L.) in Türkiye from a climate change perspective. Agriculture. 2024;14(9):1629. doi: 10.3390/agriculture14091629.

23. Al-Ghouti MA, Dib SS. Utilization of nano-olive stones in environmental remediation of methylene blue from water. J Environ Health Sci Eng. 2020;18(1):63-77. doi: 10.1007/s40201-019-00438-y.

24. Martín-Lara MA, Blázquez G, Trujillo MC, Pérez A, Calero M. New treatment of real electroplating wastewater containing heavy metal ions by adsorption onto olive stone. J Clean Prod. 2014;81:120-9. doi: 10.1016/j.jclepro.2014.06.036.

25. Al-Ghouti MA, Sweleh AO. Optimizing textile dye removal by activated carbon prepared from olive stones. Environ Technol Innov. 2019;16:100488. doi: 10.1016/j.eti.2019.100488.

26. Ahmed AM, Ali AE, Ghazy AH. Adsorption separation of nickel from wastewater by using olive stones. Adv J Chem A. 2019;2(1):79-93.

27. Amar MB, Walha K, Salvadó V. Evaluation of olive stones for Cd(II), Cu(II), Pb(II) and Cr(VI) biosorption from aqueous solution: equilibrium and kinetics. Int J Environ Res. 2020;14(2):193-204. doi: 10.1007/s41742-020-00246-5.

28. Ajmal M, Siddiq M, Aktas N, Sahiner N. Magnetic Co–Fe bimetallic nanoparticle containing modifiable microgels for the removal of heavy metal ions, organic dyes and herbicides from aqueous media. RSC Adv. 2015;5(54):43873-84. doi: 10.1039/c5ra05785j.

29. Zhou S, Dong F, Qin Y. High efficiency uranium(VI) removal from wastewater by strong alkaline ion exchange fiber: effect and characteristic. Polymers (Basel). 2023;15(2):279. doi: 10.3390/polym15020279.

30. Kim T, Shin J, An B. Adsorption characteristics for Cu(II) and phosphate in chitosan beads under single and mixed conditions. Polymers (Basel). 2023;15(2):421. doi: 10.3390/polym15020421.

31. Tong X, Li Y, Zhang F, Chen X, Zhao Y, Hu B, et al. Adsorption of 17β-estradiol onto humic-mineral complexes and effects of temperature, pH, and bisphenol A on the adsorption process. Environ Pollut. 2019;254(Pt A):112924. doi: 10.1016/j.envpol.2019.07.092.

32. Chen Z, Tang Y, Wen Q, Yang B, Pan Y. Effect of pH on effluent organic matter removal in hybrid process of magnetic ion-exchange resin adsorption and ozonation. Chemosphere. 2020;241:125090. doi: 10.1016/j.chemosphere.2019.125090.

33. El-Mas SM, Hassaan MA, El-Subruiti GM, Eltaweil AS, El Nemr A. Box-Behnken design optimization of 2D Ti3C2Tx MXene nanosheets as a microwave-absorbing catalyst for methylene blue dye degradation. Chem Eng J. 2024;500:156969. doi: 10.1016/j.cej.2024.156969.

34. Mottola S, Viscusi G, Tohamy HS, El-Sakhawy M, Gorrasi G, De Marco I. Application of electrospun N-doped carbon dots loaded cellulose acetate membranes as cationic dyes adsorbent. J Environ Manage. 2024;370:122714. doi: 10.1016/j.jenvman.2024.122714.

35. Azari A, Malakoutian M, Yaghmaeain K, Jaafarzadeh N, Shariatifar N, Mohammadi G, et al. Magnetic NH(2)-MIL-101(Al)/Chitosan nanocomposite as a novel adsorbent for the removal of azithromycin: modeling and process optimization. Sci Rep. 2022;12(1):18990. doi: 10.1038/s41598-022-21551-3.

36. Umeh AC, Hassan M, Egbuatu M, Zeng Z, Al Amin M, Samarasinghe C, et al. Multicomponent PFAS sorption and desorption in common commercial adsorbents: kinetics, isotherm, adsorbent dose, pH, and index ion and ionic strength effects. Sci Total Environ. 2023;904:166568. doi: 10.1016/j.scitotenv.2023.166568.

37. Nozari M, Malakootian M, Jaafarzadeh Haghighi Fard N, Mahmoudi-Moghaddam H. Synthesis of Fe3O4@PAC as a magnetic nano-composite for adsorption of dibutyl phthalate from the aqueous medium: modeling, analysis and optimization using the response surface methodology. Surf Interfaces. 2022;31:101981. doi: 10.1016/j.surfin.2022.101981.

38. Cheng Q, Jiang SZ, Li SQ, Wang YX, Zhang CY, Yang WR. Effects of low-dose zearalenone-contaminated diets with or without montmorillonite clay adsorbent on nutrient metabolic rates, serum enzyme activities, and genital organs of growing-laying hens. J Appl Poult Res. 2017;26(3):367-75. doi: 10.3382/japr/pfx004.

39. Asgari E, Sheikhmohammadi A, Yeganeh J. Application of the Fe3O4-chitosan nano-adsorbent for the adsorption of metronidazole from wastewater: optimization, kinetic, thermodynamic and equilibrium studies. Int J Biol Macromol. 2020;164:694-706. doi: 10.1016/j.ijbiomac.2020.07.188.

40. Rasoulzadeh H, Amir S, Esrafil A, Hashemzadeh B. The adsorption behaviour of triclosan onto magnetic bio polymer beads impregnated with diatomite. Int J Environ Anal Chem. 2023;103(16):4130-42. doi: 10.1080/03067319.2021.1922684.

41. Safari M, Rezaee R, Darvishi Cheshmeh Soltani R, Asgari E. Dual immobilization of magnetite nanoparticles and biosilica within alginate matrix for the adsorption of Cd(II) from aquatic phase. Sci Rep. 2022;12(1):11473. doi: 10.1038/s41598-022-15844-w.

42. Sheikhmohammadi A, Safari M, Alinejad A, Esrafili A, Nourmoradi H, Asgari E. The synthesis and application of the Fe3O4@SiO2 nanoparticles functionalized with 3-aminopropyltriethoxysilane as an efficient sorbent for the adsorption of ethylparaben from wastewater: synthesis, kinetic, thermodynamic and equilibrium studies. J Environ Chem Eng. 2019;7(5):103315. doi: 10.1016/j.jece.2019.103315.

43. Alsulaili A, Elsayed K, Refaie A. Utilization of agriculture waste materials as sustainable adsorbents for heavy metal removal: a comprehensive review. J Eng Res. 2024;12(4):691-703. doi: 10.1016/j.jer.2023.09.018.

44. Karić N, Maia AS, Teodorović A, Atanasova N, Langergraber G, Crini G, et al. Bio-waste valorisation: agricultural wastes as biosorbents for removal of (in)organic pollutants in wastewater treatment. Chem Eng J Adv. 2022;9:100239. doi: 10.1016/j.ceja.2021.100239.

45. Adegoke KA, Bello OS. Dye sequestration using agricultural wastes as adsorbents. Water Resour Ind. 2015;12:8-24. doi: 10.1016/j.wri.2015.09.002.